The Effect of Homogenization Heat Treatment on 316 Stainless Steel Cast Billet

Hung-Yang Chu , Ren-Kae Shiue * , Sheng-Yuan Cheng

Posted Date: 30 October 2023

doi: 10.20944/preprints202310.1829.v1

Keywords: homogenization; stainless steel; cast billet; forging; δ-ferrite; microstructure

Article

The Effect of Homogenization Heat Treatment on 316 Stainless Steel Cast Billet

Hung-Yang Chu [1], Ren-Kae Shiue [1,*] and Sheng-Yuan Cheng [2]

[1] Department of Materials Science and Engineering, National Taiwan University, Taipei 10617, Taiwan; asdf7492456@gmail.com (H.-Y.C)

[2] Stainless Steel Business Group, Walsin Lihwa Corporation, Tainan City 73743, Taiwan, R.O.C.; shengyuan_cheng@walsin.com (S.-Y.C.)

* Correspondence: rkshiue@ntu.edu.tw

Abstract: The investigation aims to analyze the effect of homogenization heat treatment on the quantity, distribution, morphology, and chemical composition of δ ferrite and sigma phase in the 316L austenitic stainless steel cast billet. Microstructures of the cast billet at different locations, center, 0.5 R, R, and the subsequent 2/6-hour homogenization heat treatment at 1240 °C were examined. The microstructure at the radius R was much more uniform and expected a better performance in the following hot/cold forging processes due to the highest cooling rate compared with those at 0.5R and center. The δ ferrite often accompanies the generation of the sigma phase, and the transformation of δ ferrite into the sigma/(austenite) and retained δ ferrite is strongly related to the cooling rate after homogenization heat treatment. The sigma phase is hard and detrimental to the subsequent hot/cold forgings. It must be removed from the homogenization heat treatment before forging. Fast air cooling from 850 °C to room temperature after homogenization heat treatment cannot prohibit the sigma phase formation. Rapid cooling between 850 and 1240 °C after homogenization treatment is required to avoid the sigma phase formation in the 316L stainless steel cast billet.

Keywords: homogenization; stainless steel; cast billet; forging; δ-ferrite; microstructure

1. Introduction

Chromium-nickel austenitic stainless steels are among the world's most widely applied engineering alloys due to their excellent formability, weldability, and corrosion resistance [1-3]. The 316L stainless steel is comprehensively used in various applications, e.g., medical supplies, fossil and nuclear power plants, petroleum refining industries, and chemical appliances due to its high ductility and strength, excellent corrosion resistance, and low cost [1,4-6]. The 316L stainless steel plate production from the cast 316L stainless billet experiences a series of hot and cold forging [7,8]. The formability of the cast billet becomes an important issue in the subsequent forging processes [9-12].

The 316L stainless steel cast billet contains Mo. It has been reported that a high content of Mo enhances the formation of Mo-rich intermetallics, such as sigma and chi phases, degrading mechanical properties and encouraging hot cracking [13,14]. Therefore, homogenization heat treatment of the cast 316L billet is necessary before hot forging the cast billet [13,15-18]. The distribution and morphology of δ-ferrite and sigma phases in the austenite matrix of the 316L cast billet are strongly related to following hot/cold forging of the cast billet. The homogenization heat treatment is expected to provide a driving force to break up the interdendritic δ-ferrite and promote the formation of spheroidal δ-ferrite in the austenite matrix. Uniformly distributed spheroidal δ-ferrite in the 316L cast billet benefits the formability of hot/cold forging.

Thermo-Calc provides the first approximation in the construction of multicomponent phase diagrams. With the advancement of the thermodynamic database, it has been used in industry [19]. Many researchers combine DSC (Differential Scanning Calorimetry) and Thermo-Calc calculation to relate the phase transformation temperatures of alloy to optimize the heat treatment condition before hot/cold working of the alloy [20-23]. Isothermal sections at selected temperature and phase fraction

Preprints (www.preprints.org) | NOT PEER-REVIEWED | Posted: 30 October 2023 doi:10.20944/preprints202310.1829.v1

upon cooling cycle can be readily achieved with acceptable accuracy [24]. It is a powerful tool in combination with experimental studies [25-28].

This investigation focuses on the effect of homogenization heat treatment of the 316L cast stainless steel billet. The morphology and distribution of δ ferrite and sigma phase formation in the austenite matrix of the cast billet were studied. The formation of the sigma phase in the homogenized cast billet was also clarified in the experiment.

2. Materials and Experimental Procedures

Walsin Lihwa Corporation prepared the 316SS cast billet with a diameter of 250 mm. The chemical composition in wt% of the 316L cast billet was 0.020 C, 0.131 Co, 18.149 Cr, 0.115 Cu, 1.849 Mn, 2.622 Mo, 0.046 N, 11.376 Ni, 0.025 P, 0.013 S, 0.942 Si, 0.101 V and Fe balance. The cast billet was wire-cut and machined to obtain test pieces with a cross-section of approximately 10 mm × 10 mm and 5 mm thick. For comparison, three samples, i.e., near surface, 1/2 radius, and center, were machined from the cast billet.

To evaluate the effect of homogenization heat treatment on 316SS cast billet, three types, namely, no heat treatment, 2 hours heat treatment, and 6 hours heat treatment for comparison. The test piece was placed into a tubular high-temperature vacuum furnace to avoid oxidation during the heat treatment. The homogenization heat treatment was performed at 1240 °C at a vacuum of 5×10^{-4} mbar. The heating rate of the high-temperature vacuum furnace was 20 °C/min, and the holding period was 2 and 6 hours, respectively. Different cooling rates were performed after the test pieces were homogenized at 1240 °C. Figure 1 shows two different cooling rates used in the experiment: air cooling (AC) and furnace cooling (FC). Table 1 shows all 316L specimen designations used in the study.

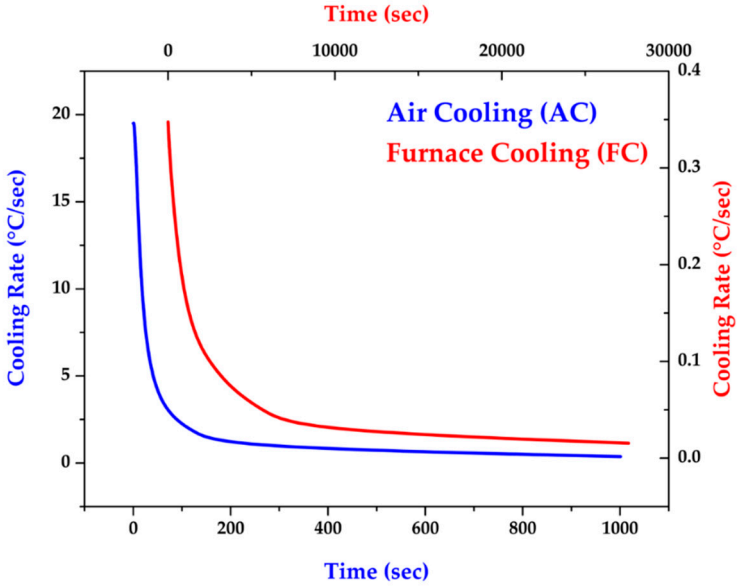

Figure 1. AC and FC cooling rates after homogenization at 1240 °C for 2 and 6 hours.

Table 1. 316L specimen designation used in the study.

Symbol	Heat Treatment	Location
C	as cast	Center
0.5R	as cast	0.5 R
R	as cast	R
C-2h-AC	1240°C for 2h, air cooling	Center
0.5R-2h-AC	1240°C for 2h, air cooling	0.5 R
R-2h-AC	1240°C for 2h, air cooling	R
C-2h-FC	1240°C for 2h, furnace cooling	Center
0.5R-2h-FC	1240°C for 2h, furnace cooling	0.5 R

Preprints (www.preprints.org) | NOT PEER-REVIEWED | Posted: 30 October 2023 doi:10.20944/preprints202310.1829.v1

R-2h-FC	1240°C for 2h, furnace cooling	R
0.5R-2h-850C-AC	1240°C for 2h, furnace cooled to 850°C, and fast air cooling	0.5 R
0.5R-6h-FC	1240°C for 6h, furnace cooling	0.5 R

All test pieces were mounted and experienced a standard metallographic procedure before inspection. A field emission scanning electron microscope (FESEM) with an electron backscatter diffraction (EBSD) was applied to perform phase identification and crystallographic analyses. A field emission electron probe microanalyzer (FE-EPMA) combined with a wavelength dispersive spectrometer (WDS) was used to perform quantitative chemical analyses of selected positions and mappings of the test pieces. Finally, a Vickers microhardness tester with a load of 10 g and 15 s duration time was used to measure the difference in hardness for various phases.

3. Results and Discussion

Figure 2 shows EBSD phase maps of the as-cast 316L stainless steel billet at different locations. The as-cast billet has three phases, including δ ferrite, sigma, and austenite. The microstructure of the three locations is quite different due to different cooling rates in casting. In Figure 2a, fragmented δ ferrite (red) is observed in the austenite (blue) matrix in the center of the cast billet. In Figure 2b, the flaky δ ferrite and sigma phase distribution is still quite uneven at 0.5 R. The distribution of flaky δ ferrite and sigma phases is improved at the location of R, as displayed in Figure 2c. In Figure 2c, the amount of sigma phase is significantly decreased, and the flaky δ ferrite becomes blunt at location R. Different microstructures of the cast billet at different locations are expected to result in different responses in the subsequent hot/cold rolling. It is required to perform a homogenization treatment of the cast billet before rolling.

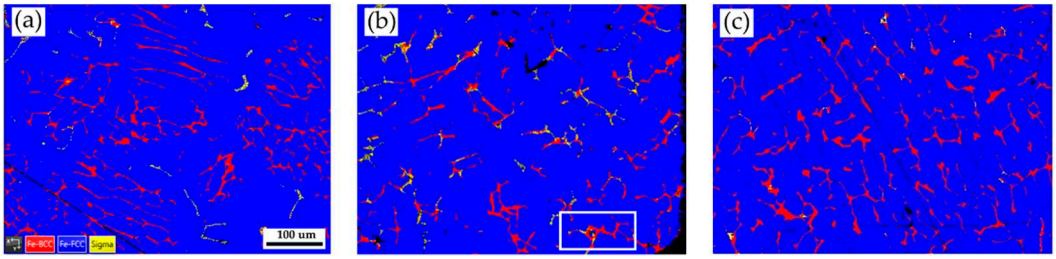

Figure 2. EBSD phase maps of the as-cast 316L stainless steel billet at different locations: (a) center, (b) 0.5 R, (c) R.

Figures 3a and 3b show EBSD phase maps of the as-cast 316L stainless steel billet at 0.5R at higher magnifications. The sigma phase (yellow) is mixed with the δ ferrite (red) in the austenite matrix (blue). The EBSD phase map in Figure 3b corresponds to the EPMA BEI displayed in Figure 3c. The EPMA WDS quantitative chemical analysis spots at different locations are shown in Figure 3c and Table 2. According to Table 2, concentrations of Cr, Mo, and Ni are pretty different in the three phases of the cast billet. The austenite is alloyed with high Ni (> 10 at%), low Mo (< 3 at%) and Cr (< 20 at%) concentrations, as marked by C, D, E, and G in Figure 3c. In contrast, the δ ferrite and sigma phases are alloyed with a low concentration of Ni (< 5 at%) and a high concentration of Cr (> 25 at%) as marked by B, F, H ~ L in Figure 3c. The Cr concentrations of the δ ferrite and sigma phases are similar, approximately between 25 and 29 at%. However, Mo concentration in the sigma phase is higher than in the δ ferrite, as displayed in Table 3. It has been reported that the presence of Mo is attributed to the formation of the sigma phase in the stainless [29]. It is consistent with the experimental result.

Preprints (www.preprints.org) | NOT PEER-REVIEWED | Posted: 30 October 2023 doi:10.20944/preprints202310.1829.v1

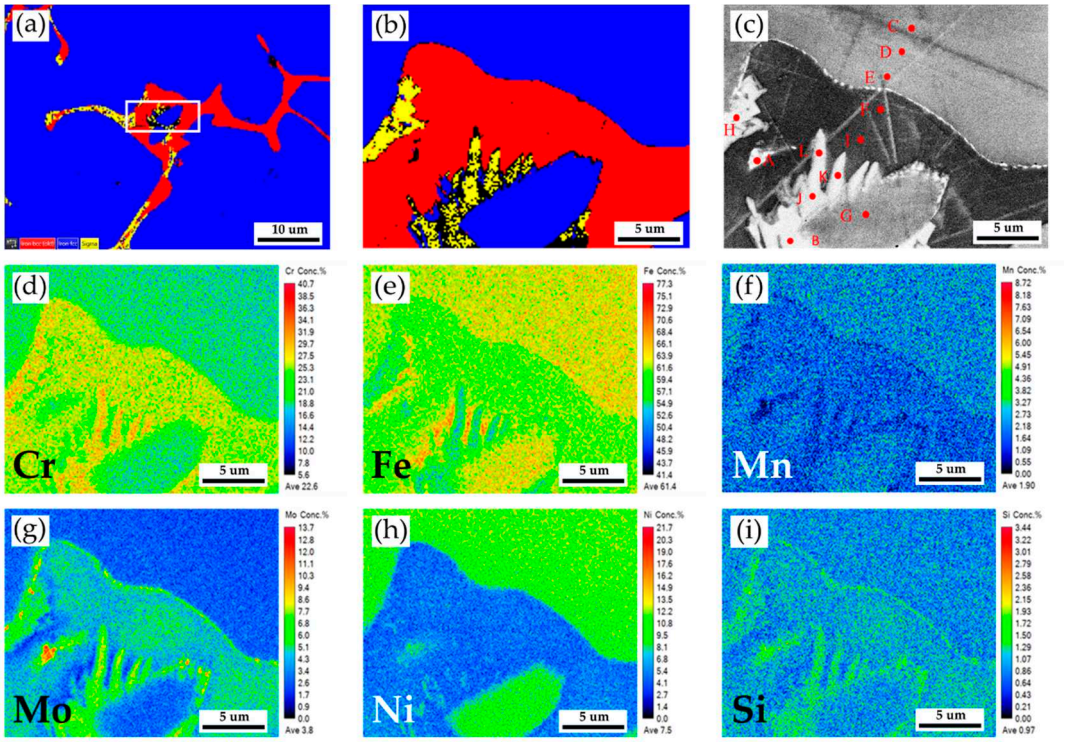

Figure 3. The as-cast 316L stainless steel billet at 0.5R: (a, b) EBSD phase maps in selected areas in Fig. 2b, (c) EPMA BEI and quantitative chemical analyses of different locations, (d~i) EPMA WDS quantitative element mappings of Cr, Fe, Mn, Mo, Ni, and Si.

Table 2. EPMA WDS quantitative chemical analyses in at% of A~-L in Figure 3c.

Element /wt%	C	Cr	Fe	Mn	Mo	Ni	O	P	Si	Si	Phase
A	0.9	21.1	56.7	1.9	10.4	7.3	0.0	0.3	0.1	1.3	---
B	0.8	28.2	56.1	1.5	7.5	4.6	0.0	0.1	0.0	1.2	sigma
C	0.2	17.7	65.4	1.9	2.2	11.8	0.0	0.0	0.0	0.8	austenite
D	1.2	18.1	64.2	2.0	2.4	11.2	0.0	0.0	0.0	0.9	austenite
E	1.1	18.7	64.2	2.0	2.6	10.5	0.0	0.0	0.0	0.9	austenite
F	0.9	25.8	60.6	1.6	5.1	4.8	0.0	0.1	0.0	1.1	δ ferrite
G	0.8	19.1	64.4	1.9	2.7	10.2	0.0	0.0	0.0	0.9	austenite
H	1.1	27.7	57.7	1.7	6.2	4.3	0.0	0.1	0.0	1.2	sigma
I	0.8	26.2	61.2	1.6	4.5	4.6	0.0	0.1	0.0	1.0	δ ferrite
J	2.1	28.2	54.9	1.6	7.1	4.6	0.0	0.1	0.2	1.2	sigma
K	2.1	26.7	56.9	1.6	6.4	4.9	0.0	0.1	0.1	1.2	sigma
L	2.1	27.9	54.7	1.6	7.5	4.5	0.0	0.2	0.2	1.3	sigma

Figure 4 and Table 3 show Vickers hardness measurement results of the as-cast 316L stainless steel billet at 0.5 R. The EBSD phase map in Figure 4a corresponds to the optical microscope image with Vickers hardness dents in Figure 4b. The austenite has the lowest hardness below 200 Hv, as illustrated by A1 ~ A3. The hardness of δ ferrite, above 200 Hv, is greater than that of austenite, as shown by B1 ~ B4. The sigma phase has the highest hardness among all phases. However, a considerable variation is observed in the hardness measurement of the sigma phase, as shown in C1 ~ C3. The hardness values of the sigma phase are between 314 and 487. Because the size of the sigma phase is less than that of Vickers hardness dent under the applied load of 10 g, both sigma and δ ferrite are covered by the hardness dent, as shown in Figure 4e. In Figure 4e, the hardness dent at location C1 covers the most significant fraction of the white sigma phase, and it has the highest Vickers hardness of 487. It is confirmed that the sigma phase has the highest hardness in the cast billet.

Preprints (www.preprints.org) | NOT PEER-REVIEWED | Posted: 30 October 2023 doi:10.20944/preprints202310.1829.v1

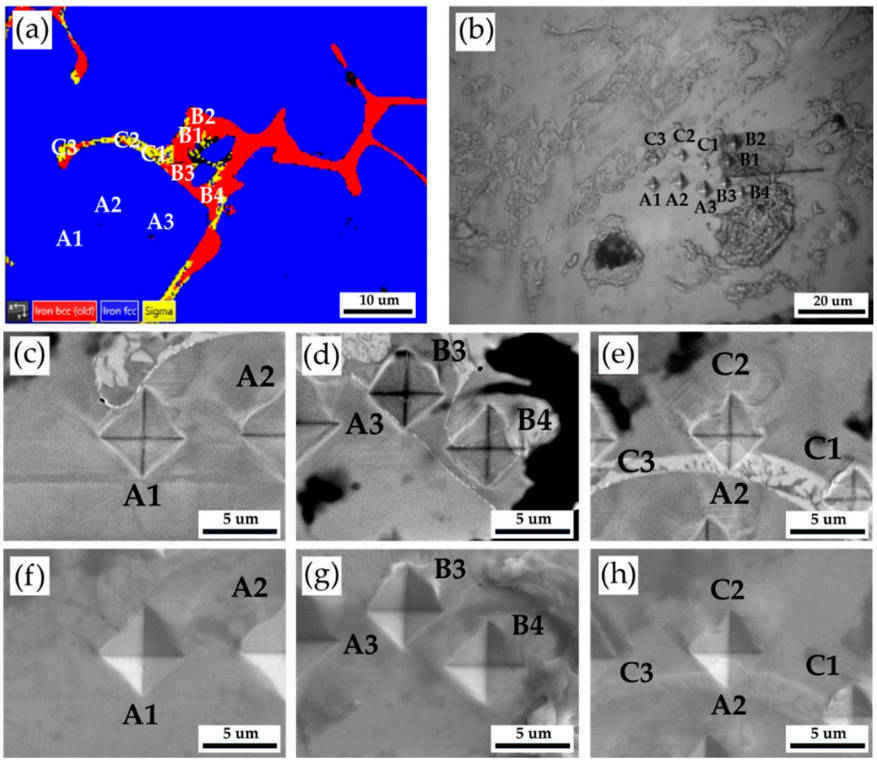

Figure 4. The Vickers hardness measurements of the as-cast 316L stainless steel billet at 0.5 R: (a) EBSD phase map in the selected area in Figure 3a, (b) the corresponding optical microscope image with Vickers hardness dents of Figure 4a, Vickers hardness dents of EPMA (c ~ e) BEIs, (f ~ h) SEIs.

Table 3. Vickers hardness measurements displayed in Figure 4.

Location	A1	A2	A3	B1	B2	B3	B4	C1	C2	C3
Hv (10 g)	1	1	1	2	2	2	2	4	3	3
	9	7	8	0	1	5	6	8	1	2
	6	1	4	0	4	1	0	7	4	8

Figure 5 shows EBSD phase maps of the 316L stainless steel cast billet after homogenization at 1240 °C for 2 hours and air cooling at three locations: center, 0.5 R, and R. The sigma phase has almost disappeared from the entire cast billet. The blunting of the flaky δ ferrite is widely observed at three locations of the cast billet. However, the distribution of δ ferrite at the center and 0.5 R is still less uniform than that at R. The homogenization heat treatment effectively improves the flaky δ ferrite into a blunt one at all locations. The homogenization heat treatment shows the best effect of spheroidizing δ ferrite at the location R of the cast billet. It is worth mentioning that the fast air cooling of the cast billet after 1240 °C for 2h homogenization heat treatment is beneficial to avoid the formation of the sigma phase in the entire 316L cast billet.

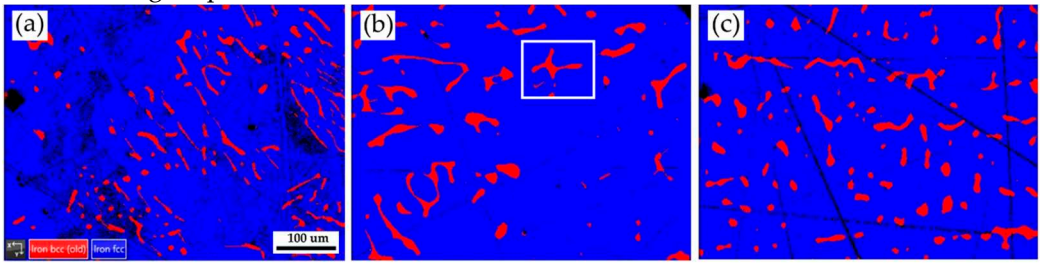

Figure 5. EBSD phase maps of the 316L stainless steel cast billet after homogenization at 1240 °C for 2 hours with air cooling at different locations: (a) C-2h-AC, (b) 0.5 R-2h-AC, (c) R-C-2h-AC.

Preprints (www.preprints.org) | NOT PEER-REVIEWED | Posted: 30 October 2023 doi:10.20944/preprints202310.1829.v1

Figure 6a displays EBSD phase maps of the 316L stainless steel cast billet after homogenization at 1240 °C for 2 hours and air cooling at 0.5 R at higher magnifications. The sigma phase disappeared from the figure due to the fast air cooling after homogenization. The area I of the EBSD phase map in Figure 6a corresponds to the EPMA BEI displayed in Figure 6b. The EPMA WDS quantitative chemical analysis spots at different locations are shown in Figure 6b and Table 3. Similar to the results above, the austenite is alloyed with high Ni (> 10 at%), low Mo (< 3 at%) and Cr (< 20 at%) concentrations, as marked by M, P, and R in Figure 6b. On the other hand, the δ ferrite is alloyed with a low concentration of Ni (< 7.4 at%) and a high concentration of Cr (> 21.9 at%) as marked by N, O, and Q in Figure 6b. The Mo concentration in the δ ferrite is slightly higher than in the austenite, as shown in Table 3. Figures 6c ~ 6h are EPMA WDS quantitative element mappings of Cr, Fe, Mn, Mo, Ni, and Si, consistent with Table 3. It is noted that the Cr and Mo are enriched in the δ ferrite close to the interface between the δ ferrite and austenite. The δ ferrite alloyed with high Cr and Mo concentrations favors the sigma phase formation and will be discussed later.

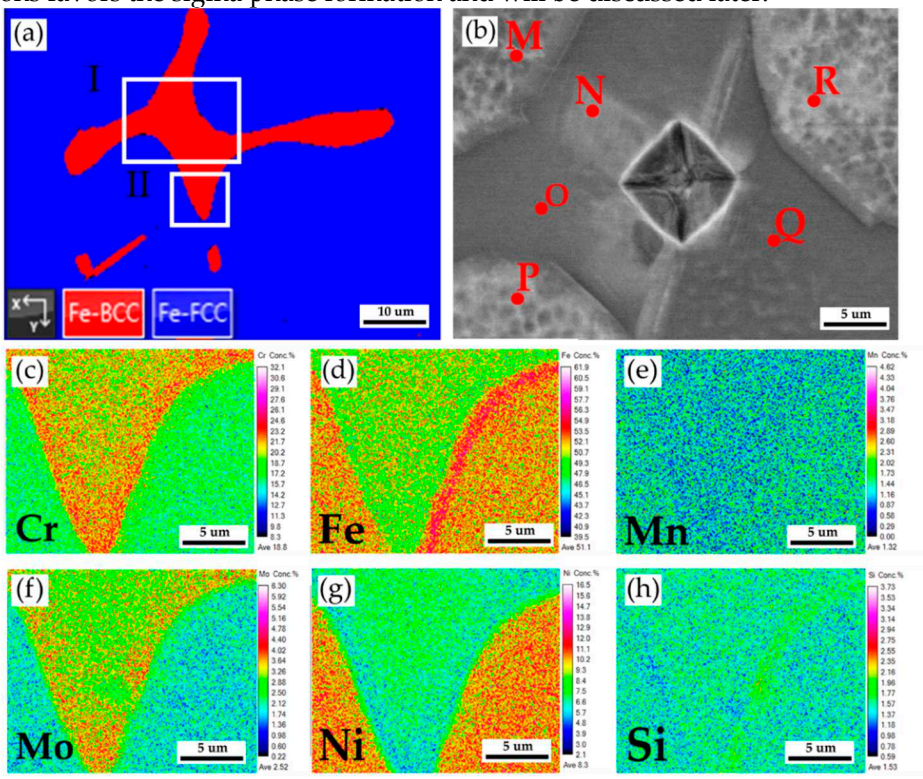

Figure 6. The cast 316L stainless steel billet at 0.5 R after homogenization at 1240 °C for 2 hours with air cooling: (a) EBSD phase map in selected area of Fig. 5b, (b) EPMA BEI and quantitative chemical analyses of different locations in area I of Figure 6a, (c~h) EPMA WDS quantitative element mappings of Cr, Fe, Mn, Mo, Ni, and Si in the area II of Figure 6a.

Table 4. EPMA WDS quantitative chemical analyses in at% of M~ R in Figure 6b.

Element /at%	C	Cr	Fe	Mn	Mo	Ni	O	P	Si	Si	Phase
M	0.1	18.8	65.4	1.5	2.4	10.9	0.0	0.0	0.1	0.8	austenite
N	0.2	23.7	62.6	1.2	4.1	7.1	0.0	0.1	0.1	0.9	δ ferrite
O	0.2	23.6	62.6	1.4	4.1	6.9	0.0	0.1	0.1	1.0	δ ferrite
P	0.1	18.3	65.8	1.4	2.4	11.1	0.0	0.0	0.1	0.8	austenite
Q	0.2	21.9	64.1	1.3	3.9	7.4	0.0	0.1	0.1	1.0	δ ferrite
R	0.2	18.1	65.6	1.5	2.5	11.1	0.0	0.0	0.1	0.9	austenite

Figure 7 and Table 5 display the Vickers hardness measurements of the as-cast 316L stainless steel billet at 0.5 R after homogenization at 1240 °C for 2 hours and air cooling. The EBSD phase map in Figure 7a corresponds to the EPMA SEI with Vickers hardness dents in Figure 7b. The hardness of

Preprints (www.preprints.org) | NOT PEER-REVIEWED | Posted: 30 October 2023 doi:10.20944/preprints202310.1829.v1

austenite is below 200 Hv. The hardness of δ ferrite is higher than 200 Hv, i.e., between 200 and B7. The homogenization heat treatment does not significantly change the hardness of austenite and δ ferrite compared to Table 3 and Table 5.

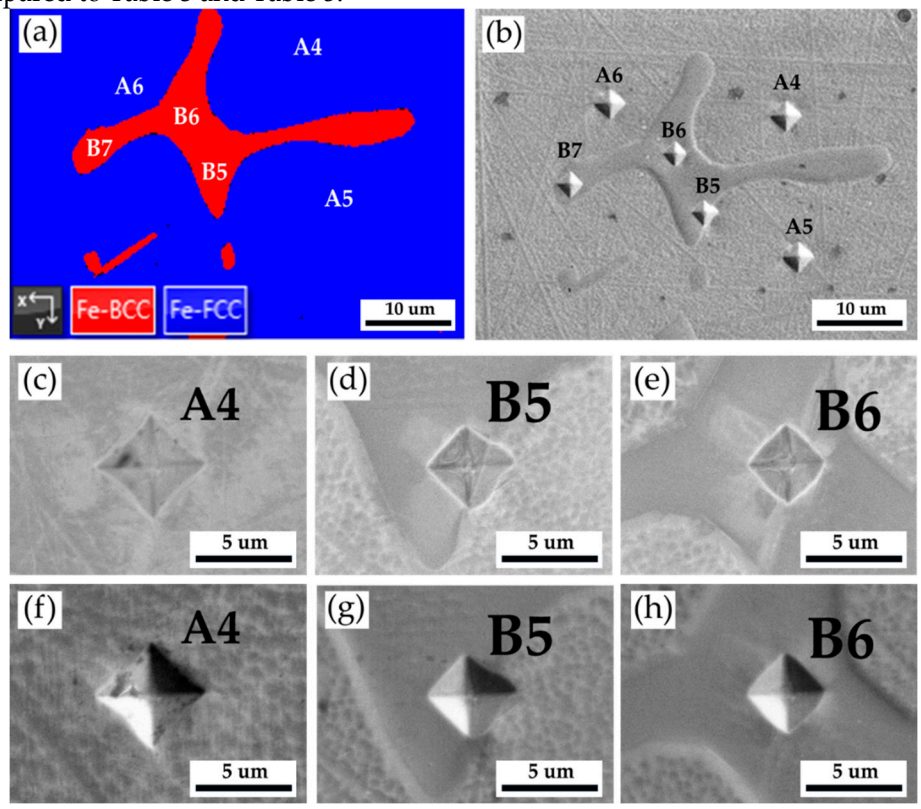

Figure 7. The Vickers hardness measurements of the as-cast 316L stainless steel billet at 0.5 R after homogenization at 1240 °C for 2 hours with air cooling: (a) EBSD phase map in the selected area in Figure 6a, (b) the corresponding EPMA SEI with Vickers hardness dents of Figure 7a, Vickers hardness dents of EPMA (c ~ e) BEIs, (f ~ h) SEIs.

Table 5. Vickers hardness measurements displayed in Figure 7.

Location	A4	A5	A6	B5	B6	B7
Hv (10 g)	196	171	184	200	214	251

Figure 8 shows the EBSD phase map of the 316L stainless steel cast billet after homogenization at 1240 °C for 2 hours and furnace cooling at location 0.5 R. The blunting of the flaky δ ferrite shown in Figure 8 is not apparent in the slow furnace cooling condition compared to the fast air cooling one, as shown in Figure 5b. A slow furnace cooling rate also forms a vast amount of sigma phase in the cast billet. According to Figure 8, many δ ferrite islands are partially transformed into the sigma phase, and only a few blocky δ ferrites are left in the austenite matrix. Figure 9a is the EBSD phase map of the selected area in Figure 8, and Figure 9b is the EBSD phase map at a higher magnification than Figure 9a. Figure 9b shows a mixture of blue austenite, red δ ferrite, and yellow sigma phases in the original δ ferrite island. The original δ ferrite has partially decomposed into an austenite and sigma phases. Figure 9c and Table 6 display EPMA BEI and quantitative chemical analyses of different locations. The austenite is alloyed with high Ni (> 10 at%), low Mo (< 3 at%) and Cr (< 19 at%) concentrations, as marked by S and X in Figure 9c. Both δ ferrite and sigma phases have low Ni (< 5 at%) and high Cr (> 20 at%) concentrations, as observed by T, U, V, and W in Figure 9c. However, the sigma phase is alloyed with the highest Cr (> 26 at%) and Mo (> 7 at%) concentrations, as displayed in Table 6. Figures 9d ~ 9i display EPMA WDS quantitative element mappings of Cr, Fe, Mn, Mo, Ni,

Preprints (www.preprints.org) | NOT PEER-REVIEWED | Posted: 30 October 2023 doi:10.20944/preprints202310.1829.v1

and Si at the identical location of Figure 9c. The white sigma phase shown in Figure 9c coincides with the Cr and Mo mappings in Figures 9d and 9g. The combination of high Cr/Mo concentrations and slow furnace cooling favors the sigma phase formation.

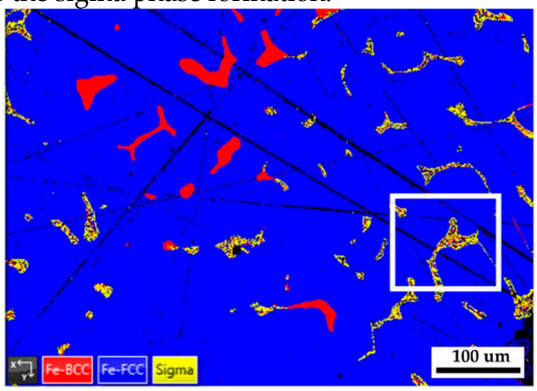

Figure 8. The EBSD phase map of the 316L stainless steel cast billet after homogenization at 1240 °C for 2 hours with furnace cooling at location 0.5 R.

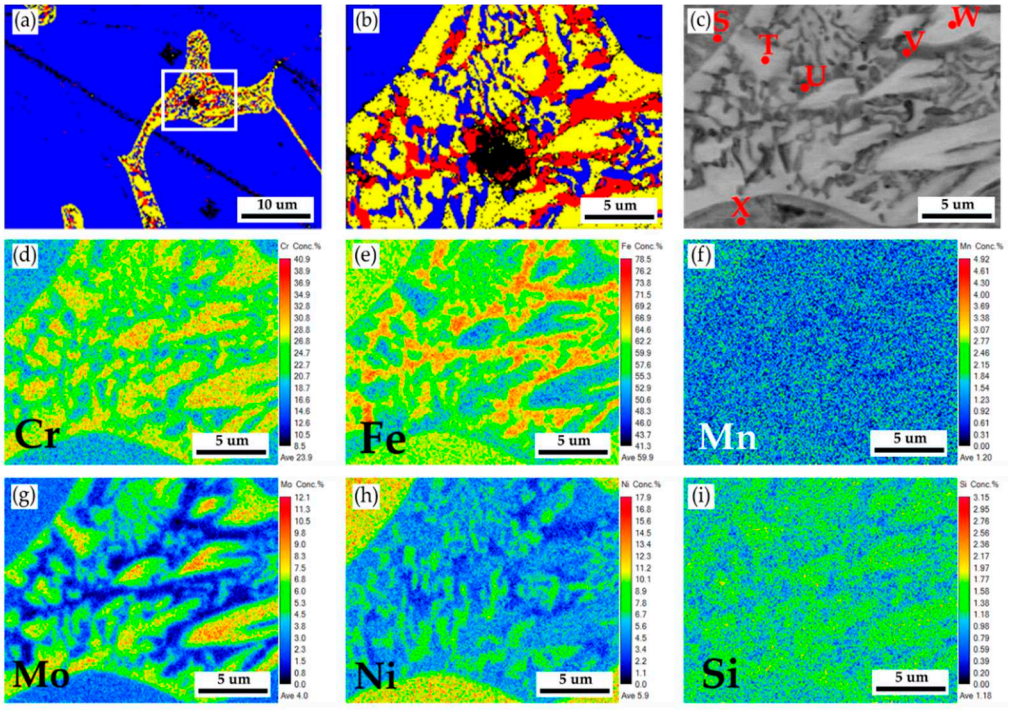

Figure 9. The cast 316L stainless steel billet at 0.5 R after homogenization at 1240 °C for 2 hours with furnace cooling: (a, b) EBSD phase maps in selected areas in Fig. 8, (c) EPMA BEI and quantitative chemical analyses of different locations, (d~i) EPMA WDS quantitative element mappings of Cr, Fe, Mn, Mo, Ni, and Si.

Table 6. EPMA WDS quantitative chemical analyses in at% of S~X in Figure 9c.

Element /at%	C	Cr	Fe	Mn	Mo	Ni	O	P	Si	Si	Phase
S	0.1	18.6	65.2	1.3	2.6	11.2	0.0	0.0	0.1	0.9	austenite
T	0.1	28.2	56.7	1.2	7.6	4.7	0.0	0.1	0.2	1.2	sigma
U	0.1	21.1	73.7	0.8	1.0	2.6	0.0	0.0	0.0	0.7	δ ferrite
V	0.2	20.9	74.1	0.8	0.8	2.5	0.0	0.0	0.0	0.7	δ ferrite
W	0.1	26.2	58.8	1.2	7.7	4.5	0.0	0.1	0.2	1.2	sigma
X	0.1	17.3	67	1.3	2.6	10.7	0.0	0.0	0.1	0.9	austenite

Figure 10 and Table 7 show the Vickers hardness measurements of the as-cast 316L stainless steel billet at 0.5 R after homogenization at 1240 °C for 2 hours and slow furnace cooling. The

Preprints (www.preprints.org) | NOT PEER-REVIEWED | Posted: 30 October 2023 doi:10.20944/preprints202310.1829.v1

corresponding EPMA SEIs/BEIs with Vickers hardness dents of Figure 10a are also included to validate the locations of different phases in the hardness test. The hardness of austenite is quite soft, below 200 Hv, similar to the result above. In contrast, the hardness of δ ferrite is significantly increased up to 402 Hv, as compared with that in Tables 3 and 5. Because the δ ferrite hardness is seldom above 300 Hv, the preliminary transformation could occur in the δ ferrite grains. The sigma phase has the highest Vickers hardness of 741. The high hardness of the sigma phase is detrimental to the subsequent hot/cold forging of the 316L cast billet. It has better be removed before the following forging process.

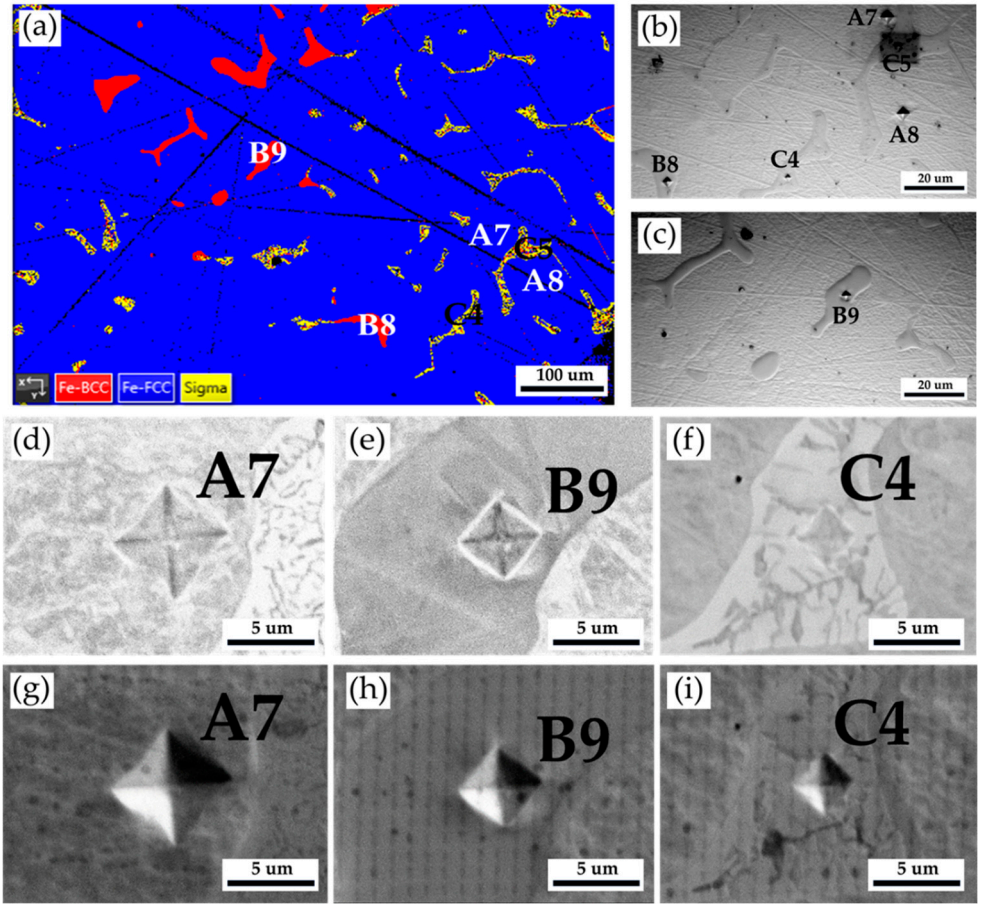

Figure 10. The Vickers hardness measurements of the as-cast 316L stainless steel billet at 0.5 R after homogenization at 1240 °C for 2 hours with furnace cooling: (a) EBSD phase map in Figure 8, (b, c) the corresponding optical metallographs with Vickers hardness dents of Figure 10a, Vickers hardness dents of EPMA (d ~ f) BEIs, (g ~ i) SEIs.

Table 7. Vickers hardness measurements displayed in Figure 10.

Location	A7	A8	B8	B9	C4	C5
Hv (10 g)	173	179	363	402	691	741

Figure 11 displays EBSD phase maps of the 316L stainless steel cast billet after homogenization at 1240 °C for 6 hours and furnace cooling at location 0.5 R. The microstructure with 6-hour homogenization illustrated in Figure 11 is similar to that in Figure 8 with 2-hour homogenization. The blunting of the flaky δ ferrite with slow furnace cooling conditions shown in Figures 8 and 11 is inferior to that in Figure 5b with the fast air cooling one. The extension of homogenization time at

Preprints (www.preprints.org) | NOT PEER-REVIEWED | Posted: 30 October 2023 doi:10.20944/preprints202310.1829.v1

1240 °C from 2 to 6 hours has little effect on the microstructure of the 316L cast billet. Figures 12a and 12b show EBSD phase maps of selected areas in Fig. 11. The original flaky δ ferrite islands could transform into a mixture of austenite, sigma, and retained δ ferrite, as illustrated in Figure 12b. Figure 12c is the corresponding EPMA BEI of Figure 12b, and quantitative chemical analyses of different locations in Figure 12c are displayed in Table 8. The sigma phase has high Cr and Mo concentrations marked by a, b, and c in Figure 12c. The austenite is alloyed with low Cr and high Ni concentrations, as marked by Y and Z. It is important to note that the δ ferrite is alloyed with deficient Mo concentration below 1.0 at%, as denoted by d, e, and f in Figure 12c. The transformation of δ ferrite into the sigma phase results from the enrichment of the Mo in the sigma phase. Migration of Mo in the original δ ferrite plays an important role in forming the sigma phase. Figures 12d ~ 12i show EPMA WDS quantitative element mappings of Cr, Fe, Mn, Mo, Ni, and Si. The sigma phase is rich in Cr and Mo, as demonstrated in Figures 12d and 12g. The austenite is rich in Ni, as displayed in Figure 12h. They are all consistent with the EPMA analysis results.

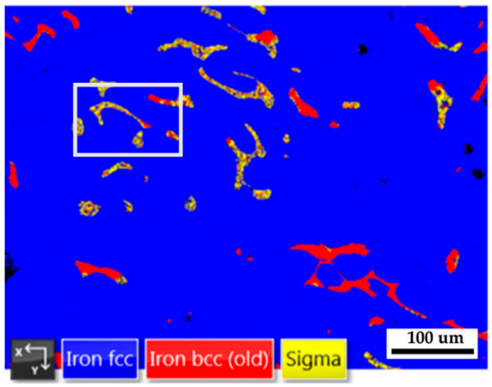

Figure 11. The EBSD phase map of the 316L stainless steel cast billet after homogenization at 1240 °C for 6 hours with furnace cooling at location 0.5 R.

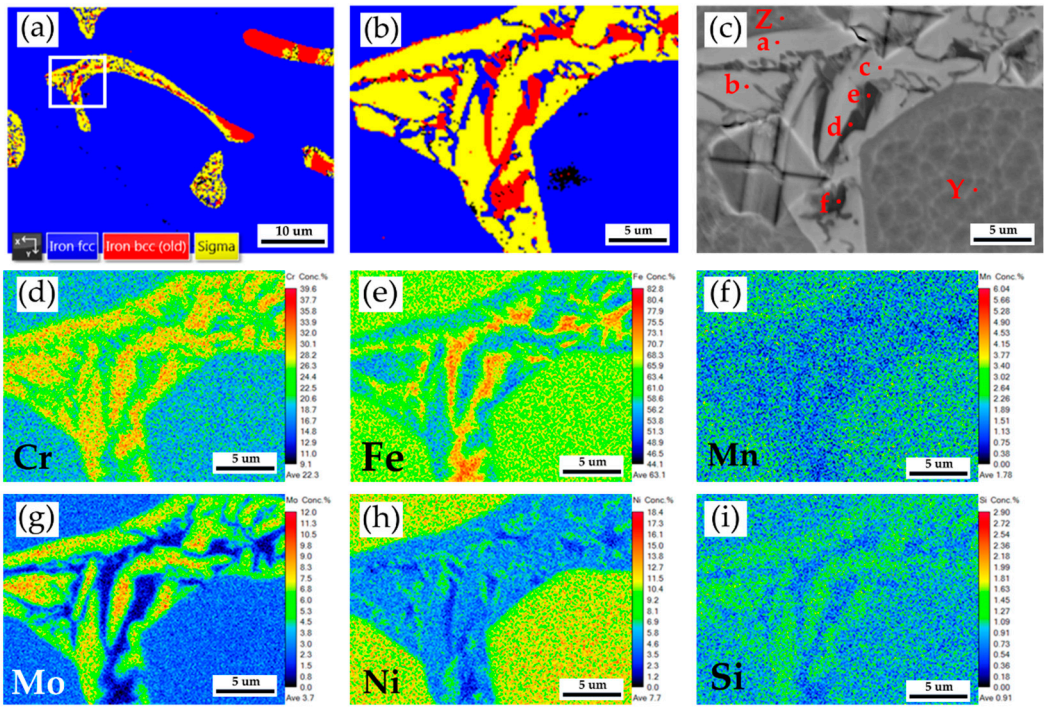

Figure 12. The cast 316L stainless steel billet at 0.5 R after homogenization at 1240 °C for 6 hours with furnace cooling: (a, b) EBSD phase maps in selected areas in Fig. 8, (c) EPMA BEI and quantitative chemical analyses of different locations, (d~i) EPMA WDS quantitative element mappings of Cr, Fe, Mn, Mo, Ni, and Si.

Preprints (www.preprints.org) | NOT PEER-REVIEWED | Posted: 30 October 2023 doi:10.20944/preprints202310.1829.v1

Table 8. EPMA WDS quantitative chemical analyses in at% of Y~f in Figure 12c.

Element /at%	C	Cr	Fe	Mn	Mo	Ni	O	P	Si	Si	Phase
Y	0.5	18.3	64.5	1.9	2.4	11.3	0.0	0.0	0.1	1.0	austenite
Z	0.5	18.6	64.4	1.9	2.5	11.0	0.0	0.0	0.1	1.0	austenite
a	0.5	29.0	55.6	1.6	7.4	4.5	0.0	0.1	0.2	1.1	sigma
b	0.5	28.6	55.2	1.7	7.6	4.9	0.0	0.1	0.2	1.2	sigma
c	0.6	28.6	55.9	1.7	6.8	5.0	0.0	0.1	0.1	1.2	sigma
d	0.5	20.9	71.7	1.2	0.8	4.2	0.0	0.0	0.0	0.7	δ ferrite
e	0.5	23.6	69.6	1.1	1.0	3.2	0.0	0.0	0.0	1.0	δ ferrite
f	0.6	21.2	73.5	1.0	0.5	2.6	0.0	0.0	0.0	0.6	δ ferrite

Figure 13 and Table 9 are Vickers microhardness test results of the cast 316L stainless steel billet at 0.5 R after homogenization at 1240 °C for 6 hours with slow furnace cooling. Figure 13a shows the EBSD phase map at the selected area in Figure 11a, and Figure 13b displays the corresponding optical metallograph with Vickers hardness dents of Figure 13a. Vickers hardness dents of EPMA SEIs (Figures 13c ~ 13e) and BEIs (Figures 13f ~ 13h) SEIs are also included in the figure. The hardness of austenite is the softest phase below 200 Hv. The hardness of δ ferrite is higher than that of austenite. The sigma phase has the highest hardness value of 860 Hv. The presence of high-hardness sigma intermetallics is detrimental to the subsequent forging of the 316L cast billet.

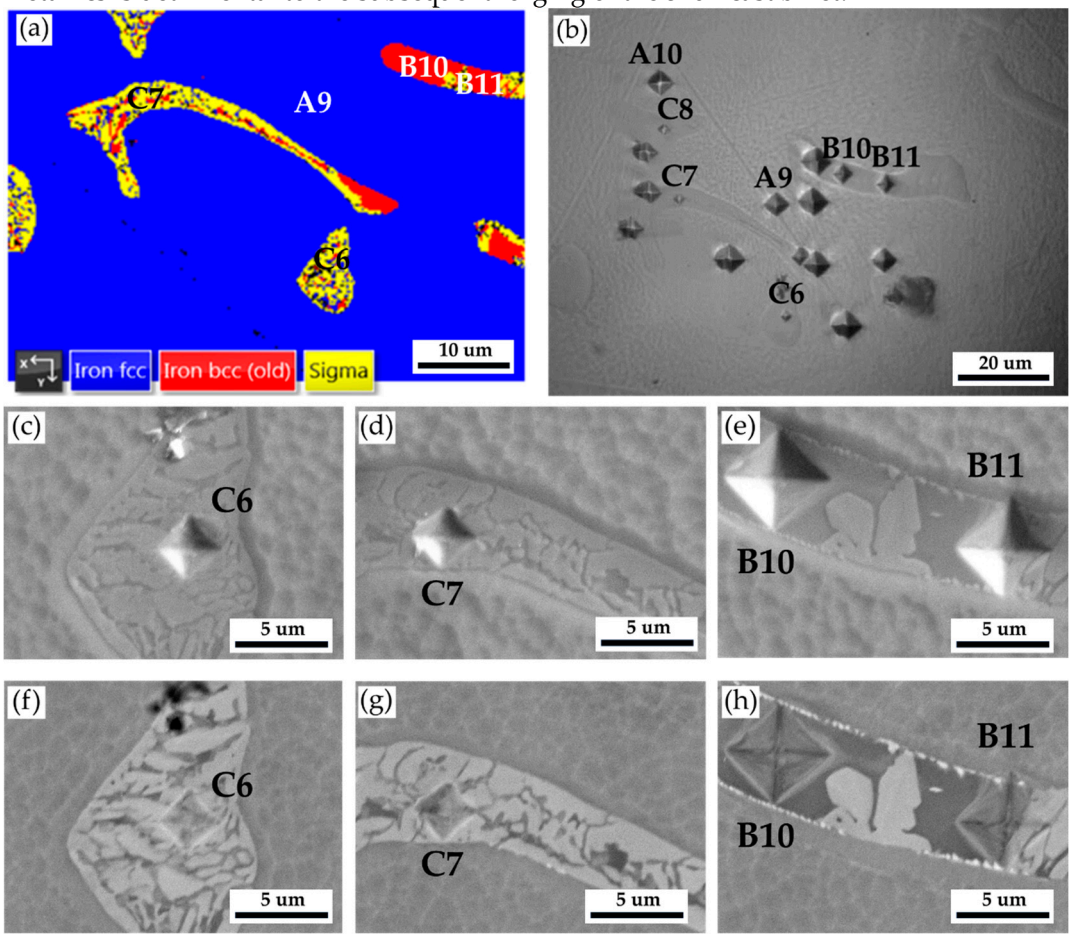

Figure 13. The Vickers hardness measurements of the as-cast 316L stainless steel billet at 0.5 R after homogenization at 1240 °C for 6 hours with furnace cooling: (a) EBSD phase map, (b) the corresponding optical metallograph with Vickers hardness dents of Figure 13a, Vickers hardness dents of EPMA (c ~ e) SEIs, (f ~ h) BEIs.

Table 9. Vickers hardness measurements displayed in Figure 10.

Location	A9	A1	B1	B1	C6	C7	C8
		0	0	1			

Preprints (www.preprints.org) | NOT PEER-REVIEWED | Posted: 30 October 2023 doi:10.20944/preprints202310.1829.v1

Hv (10 g)	17 3	14 2	22 3	28 7	64 6	86 0	60 5

Figure 14 shows the isothermal sections of the 316L stainless steel at 1240 and 850 °C simulated by Thermo-Calc, respectively. In Figure 14a, the chemical composition of the 316L cast billet is in the two-phase region, δ ferrite (BCC) and austenite (FCC), consistent with the experimental observation. According to Figure 14b, the equilibrium phases at 850 °C in the 316L stainless steel are FCC austenite, $M_{23}C_6$ carbide, and the sigma phase. The 316L cast billet is alloyed with a low carbon concentration of 0.02 wt%, so it is reasonable that the $M_{23}C_6$ carbide is not observed in the experiment. However, the δ ferrite is not in an equilibrium phase at 850 °C in the isothermal section (Figure 14b). It is not consistent with the experimental observation. The Thermo-Calc simulation deviates from the practical result. Because the formation of the sigma phase is a kinetic issue, i.e., a rate-dependent process, the simulation based on thermodynamics is not suitable. The Thermo-Calc simulation application is unsuitable for all temperatures, especially for the case of solid-state transformation due to slow diffusion to reach the final equilibrium state.

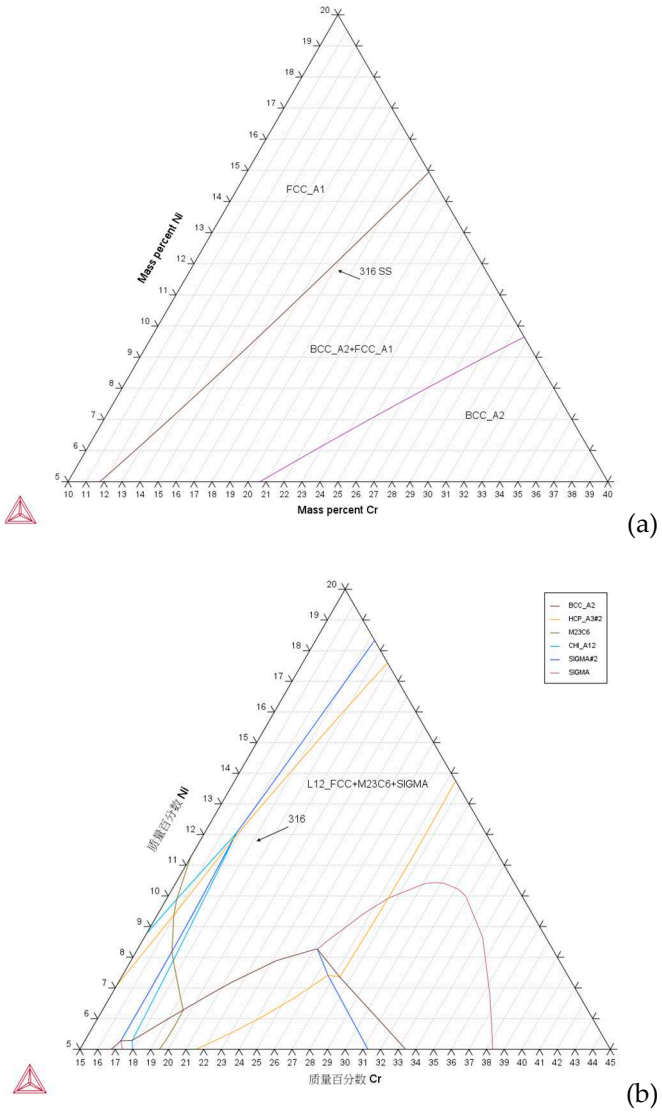

Figure 14. The isothermal sections of the 316L stainless steel at (a) 1240 and (b) 850 °C simulated by Thermo-Calc.

Figure 15 shows the EBSD phase map of the 316L stainless steel cast billet after homogenization at 1240 °C for 2 hours with a slow furnace cooled to 850 °C and followed by a fast air cooling to room temperature. The original δ ferrite islands have partially transformed into the sigma phase, a few

 doi:10.20944/preprints202310.1829.v1

austenite particles, and retained δ ferrite. The microstructure of Figure 15 is similar to those of Figures 8 and 11. Fast air cooling from 850 °C to room temperature after homogenization heat treatment cannot prohibit the sigma phase formation. In contrast, the sigma phase has almost disappeared from the entire cast billet for fast air cooling after the homogenization heat treatment at 1240 °C, as demonstrated in Figure 5. It is deduced that rapid cooling is required between 850 and 1240 °C after homogenization treatment to avoid the sigma phase formation in the 316L cast billet.

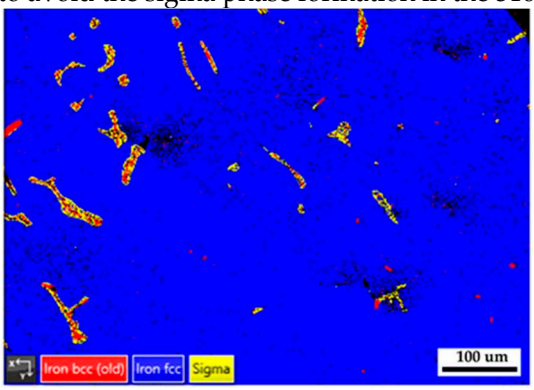

Figure 15. The EBSD phase map of the 316L stainless steel cast billet after homogenization at 1240 °C for 2 hours with a slow furnace cooled to 850 °C, followed by a fast air cooling to room temperature.

4. Conclusions

The effect of homogenization heat treatment on 316 stainless steel cast billets at 1240 °C for 2 and 6 hours has been investigated. Important conclusions are summarized below.

1. The as-cast billet consists of flaky δ ferrite accompanied by a sigma phase in the austenite matrix. The microstructure at the radius R was much more uniform than those at 0.5 R and the center of the as-cast 316L billet due to the highest cooling rate at R after casting. A better performance in the circumference of the cast billet is expected in the following forgings.
2. After homogenization treatment, the sigma phase has almost disappeared from the entire cast billet for fast air cooling. The blunting of the flaky δ ferrite is widely observed at three locations of the cast billet. However, the distribution of δ ferrite at the center and 0.5 R is still less uniform than that at R. The homogenization heat treatment effectively improves the flaky δ ferrites into blunt ones at all locations.
3. For the slow furnace cooling after homogenization heat treatment, the δ ferrite often accompanies the generation of the sigma phase. The transformation of δ ferrite into the sigma/(austenite) and retained δ ferrite is strongly related to the cooling rate after homogenization heat treatment. The sigma phase is hard and detrimental to the subsequent hot/cold forgings. It should be removed from the homogenization heat treatment before forging.
4. The microstructure with 6-hour homogenization is similar to that with 2-hour homogenization for the slow furnace cooling specimens. The blunting of the flaky δ ferrite with slow furnace cooling conditions is inferior to fast air cooling. The extension of homogenization time at 1240 °C from 2 to 6 hours has little effect on the microstructure of the 316L cast billet.
5. Fast air cooling from 850 °C to room temperature after homogenization heat treatment cannot prohibit the sigma phase formation. Rapid cooling between 850 and 1240 °C after homogenization treatment is required to avoid the sigma phase formation in the 316L cast billet.

Author Contributions: Experiment, H.-Y.C.; formal analysis, H.-Y.C., and S.-Y. C.; writing original draft preparation, R.-K.S.; writing—review and editing, R.-K. S., H.-Y.C., and S.-Y.C; funding acquisition, R.-K.S.; Resources, R.-K.S., and S.-Y. C. All authors have read and agreed to the published version of the manuscript.

Funding: This research was funded by the Walsin Lihwa Corporation, Taiwan.

Institutional Review Board Statement: Not applicable.

Informed Consent Statement: Not applicable.

Data Availability Statement: Not applicable.

Acknowledgments: Thanks to H.C. Lin, C.Y. Kao, C.S. Lin, and Y.T. Lee of the Instrumentation Center, National Taiwan University for EPMA and FEG-SEM experiments.

Conflicts of Interest: Authors declare no conflict of interest.

References

1. Astafurov, S.; Astafurova, E. Phase composition of austenitic stainless steels in additive manufacturing: a review. *Metals* **2021**, 11, 1052.
2. Lo, K.H.; Shek, C.H.; Lai, J.K.L. Recent developments in stainless steels. *Mat. Sci. Eng. R.* **2009**, 65, 39–104.
3. Bhadeshia, H.; Honeykombe, R. Steels: microstructure and properties; Elsevier, Amsterdam, The Netherlands, 2006.
4. Saeidi, K.; Gao, X.; Zhong, Y.; Shen, Z.J. Hardened austenite steel with columnar subgrain structure formed by laser melting. *Mater. Sci. Eng. A* **2015**, 625, 221–229.
5. Godec, M.; Zaefferer, S.; Podgornik, B.; Šinko, M.; Tchernychova, E. Quantitative multiscale correlative microstructure analysis of additive manufacturing of stainless steel 316L processed by selective laser melting. *Mater. Charact.* **2020**, 160, 110074.
6. Lima, M.S.F.; Sankaré, S. Microstructure and mechanical behavior of laser additive manufactured AISI 316 stainless steel stringers. *Mater. Des.* **2014**, 55, 526–532.
7. IIola, R.; Hänninen, H.; Kauppi, T. Hot and cold rolling of high nitrogen Cr-Ni and Cr-Mn austenitic stainless steels, *J. Mater. Eng. Perform.* **1998**, 7(5), 661-666.
8. Raabe, D. Overview on basic types of hot rolling textures of steels, *Steel Res. Inter.* **2003**, 74(5), 327-337.
9. Farahat, A.I.Z.; El-Bita, T.A. Effect of Nb, Ti and cold deformation on microstructure and mechanical properties of austenitic stainless steels, *Mater. Sci. Eng A* **2010**, 527, 3662-3669.
10. Czerwinski, F.; Cho, J.Y.; Brodtka, A.; Lipiec, Z.; Sunwoo, J.H.; Szpunar, J.A. The edge-cracking of AISI 304 stainless steel during hot-rolling, *J. Mater. Sci.* **1999**, 34, 4727-4735.
11. Hong, C.M.; Shi, J; Sheng, L.Y.; Cao, W.Q; Hui, W.J.; Dong, H. Influence of hot working on microstructure and mechanical behavior of high nitrogen stainless steel, *J. Mater. Sci.*, **2011**, 46, 5097-5103.
12. Raabe, D. Texture and microstructure evolution during cold rolling of a strip cast and of a hot rolled austenitic stainless steel, *Acta Mater.* **1997**, 45(3), 1137-1151.
13. Hao, Y.; Cao, G.; Li, C.; Liu, W.; Li, J.; Liu, Z.; Gao, F. Solidification structures of Fe–Cr–Ni–Mo–N super-austenitic stainless steel processed by twin-roll strip casting and ingot casting and their segregation evolution behaviors, *ISIJ Inter.* **2018**, 58(10), 1801-1810.
14. Anderson, T.D.; DuPont, J.N.; Perricone, M.J.; Marder, A.R. Phase Transformations and Microstructural Evolution of Mo-Bearing Stainless Steels, *Metall. Mater. Trans. A* **2007**, 38A, 672-685.
15. Xie, A.; Chen, S.; Wu, Y.; Jiang, H.; Rong, L. Homogenization temperature dependent microstructural evolution and mechanical properties in a Nb-stabilized cast austenitic stainless steel, *Mater. Charc.* **2022**, 194, 112384.
16. DuPont, J.N.; Farren, J.D. Influence of Heat Treatment Time and temperature on the microstructure and corrosion resistance of cast superaustenitic stainless steels, *Corrosion*, **2011**, 67(5), 055002-1–055002-11.
17. Zhang, R.; He, J.; Xu, S.; Zhang, F.; Wang, X. The optimized homogenization process of cast 7Mo super austenitic stainless steel, *Materials* **2023**, 16, 3438.
18. Zhang, R.; He, J.; Xu, S.; Zhang, F; Wang, X. Exploring the mechanism of solid-state transformation $\sigma \rightarrow \gamma$ during homogenization in 7Mo super austenitic stainless steel, *J. Mater. Res. Tech.* **2023**, 26, 999-1005.
19. Babu, S.R.; Jaskari, M; Jarvenpää, A.; Davis, T.P.; Kömi, J.; Porter, D. Precipitation versus partitioning kinetics during the quenching of low-carbon martensitic steels, *Metals* **2020**, 10, 850.
20. Wang, H.S.; Hsieh, P.J. Establishment of heat treatment process for modified 440A martensitic stainless steel using differential
21. scanning calorimetry and thermo-calc calculation, *Metals* **2016**, 6, 4.
22. Andersson, J.O.; Helander, T.; Hdghmd, L.; Shi, P.; Sundman, B. Thermo-Calc & DICTRA computational tools. *Mater. Sci.* **2002**, 26, 273–312.
23. Zhang, J.; Singer, R.F. Hot tearing of nickel-based superalloys during directional solidification. *Acta Mater.* **2002**, 50, 1869–1879.
24. Shi, Z.; Dong, J.; Zhang, M.; Zheng, L. Solidification characteristics and segregation behavior of Ni-based superalloy K418 for auto turbocharger turbine. *J. Alloy. Compd.* **2013**, 571, 168–177.
25. Wang, Q.; Cheng, G.; Hou, Y. Effect of Titanium Addition on As-Cast Structure and High-Temperature Tensile Property of 20Cr-8Ni Stainless Steel for Heavy Castings. *Metals* **2020**, 10, 529.
26. Kitashima, T. Coupling of the phase-field and CALPHAD methods for predicting multicomponent, solid-state phase transformations. *Phil. Mag.* **2008**, 88(11), 1615–1637.
27. Zargar, T.; Sadeghi, F; Kim, J.W.; Lee, J.S.; Heo, Y.U.; Yim, C.H. Kinetic model to investigate the effect of cooling rate on δ-ferrite behavior and its application in continuous casting of AISI 304 stainless steel. *Metals Mater. Inter.* **2022**, 28, 2263-2276.

28. Jablonski, P.D.; Hawk, J.A. Homogenizing advanced alloys: thermodynamic and kinetic simulations followed by experimental results. *J. Mater. Eng. Per.* **2017**, 26, 4-13.
29. Morais, L.C.; Magnabosco, R. Experimental investigations and DICTRA® simulation of sigma phase formation in a duplex stainless steel, *CALPHAD* **2017**, 58, 214–218.